

## Agglomeration and sintering in annealed FePt nanoparticle assemblies studied by small angle neutron scattering and x-ray diffraction

T. Thomson,<sup>1</sup> S. L. Lee,<sup>2</sup> M. F. Toney,<sup>3</sup> C. D. Dewhurst,<sup>4</sup> F. Y. Ogrin,<sup>5</sup> C. J. Oates,<sup>2</sup> and S. Sun<sup>6</sup>

<sup>1</sup>*Hitachi San Jose Research Center, 650 Harry Road, San Jose, California 95120, USA*

<sup>2</sup>*School of Physics and Astronomy, University of St. Andrews, St. Andrews, Fife KY16 9SS, United Kingdom*

<sup>3</sup>*Stanford Synchrotron Radiation Laboratory, Stanford Linear Accelerator Center, 2575 Sand Hill Road, Menlo Park, California 94025, USA*

<sup>4</sup>*Institut Laue Langevin, 38042 Grenoble, France*

<sup>5</sup>*School of Physics, University of Exeter, Exeter EX4 4QL, United Kingdom*

<sup>6</sup>*IBM—T.J. Watson Research Center, Yorktown Heights, New York 10598, USA*

(Received 17 September 2004; revised manuscript received 29 April 2005; published 19 August 2005)

In this work we give a detailed account of complementary small angle neutron scattering and x-ray diffraction studies of polymer mediated, self-assembled FePt nanoparticle arrays as a function of annealing temperature. The combination of these two techniques provides significantly greater physical insight than is available using either individually. Since both methods integrate over a large number of particles statistically meaningful data can be obtained in contrast to imaging techniques where typically only small areas are analyzed. The data show that the median particle size increases with annealing at temperatures of 580 °C and above. The data also demonstrate that the distribution of particle diameters is significant and increases with annealing temperature. These results allow a comprehensive structural model of the annealed assemblies to be developed in terms of particle sintering and agglomeration. This enhanced understanding will allow new strategies to be pursued in realizing the potential of nanoparticle assemblies as a monodispersed data storage medium.

DOI: [10.1103/PhysRevB.72.064441](https://doi.org/10.1103/PhysRevB.72.064441)

PACS number(s): 75.50.Tt, 61.12.Ex, 75.75.+a, 75.50.Bb

### I. INTRODUCTION

$L1_0$  phase, high magnetic anisotropy nanoparticles comprised of equiatomic FePt are attracting considerable attention<sup>1–11</sup> due to their potential in future nanomagnetic devices. Possible applications for magnetic nanoparticles include their use as permanent magnets,<sup>2</sup> biosensors,<sup>12</sup> biomedical applications,<sup>13</sup> and drug delivery systems.<sup>14</sup> However, the initial work on high anisotropy nanoparticles has focused on their potential application as a data storage medium<sup>15–20</sup> with the ultimate goal of storing one data bit per particle giving an areal density of approximately 40 Tbit/in.<sup>2</sup>. The high anisotropy found in chemically ordered  $L1_0$  materials<sup>21</sup> implies that nanoparticles with diameters of less than 3 nm will have sufficient anisotropy to be magnetically stable at room temperature.

Solution-phase synthesis of nanoparticles has shown that particles with diameters of 4 nm and very narrow size distributions (rms/mean=0.05) can be produced.<sup>1</sup> The particles are then deposited, via self-assembly, onto Si substrates to form an ordered thin film array. The self-assembly technique allows good control over the arrangement of particles on the substrate, over lateral dimensions of microns. However, the as-deposited particles are not in the chemically ordered, high anisotropy  $L1_0$  phase and are typically observed to have only a small saturation magnetization ( $M_s$ ) and zero coercivity ( $H_c$ ) at room temperature. In order to convert the as-deposited nanoparticles into the  $L1_0$  phase it is necessary to anneal at temperatures above 500 °C. Annealing at these temperatures allows the possibility of individual nanoparticles agglomerating to form clusters. Other workers have recently reported that the temperature at which the onset of

ordering occurs can be reduced through the use of dopants such as Cu,<sup>22</sup> Ag, or Au.<sup>23,24</sup> Since one of the main attractions of nanoparticle arrays as a data storage medium is the monodisperse nature of the particles, we concentrate in this work on describing the interparticle changes that occur when arrays, consisting of three polymer mediated, self-assembled layers deposited onto Si substrates, are annealed. Combining results from small angle neutron scattering (SANS), x-ray diffraction (XRD), and magnetization measurements allows a comprehensive structural model of unannealed nanoparticle arrays to be developed. We use this as a starting point to show that at the temperatures required to create the  $L1_0$  phase, agglomeration always occurs in our samples and that the effect is more severe the higher the annealing temperature used.

### II. EXPERIMENT

FePt nanoparticles were prepared using an arrested precipitation, solution chemistry approach. Thin film assemblies were then created by depositing the particles onto Si substrates, polished on both sides, using the polymer mediated, layer-by-layer technique described previously.<sup>25,26</sup> This resulted in films consisting of three layers of 4 nm  $\text{Fe}_{58}\text{Pt}_{42}$  self-assembled particles. The composition of  $\text{Fe}_{58}\text{Pt}_{42}$  was chosen as it had been shown previously to exhibit the highest coercivity.<sup>1,26</sup> The polymer-mediated approach results in nanoparticles with an extremely narrow size distribution, typically rms/mean < 5%, and a well-defined periodicity. The as-deposited films were annealed under nitrogen at atmospheric pressure over a range of temperatures from 580 to 800 °C. All samples were annealed for 5 min except

at the lowest temperature where they were annealed for 30 min. This difference in time is not critical for an anneal temperature of 580 °C and so we treat this series of samples as an annealing temperature series.

A subset of the annealed films was studied using the D11 diffractometer<sup>27</sup> at the ILL in Grenoble, France using a neutron wavelength of  $\lambda=0.45$  nm. The neutrons were collimated to give a beam diameter of 16 mm. Data were collected at three detector positions in order to scan a  $\mathbf{q}$  range of  $0.12\text{--}3.0$  nm<sup>-1</sup>. The small volume of material meant that it was necessary to stack a number of samples to increase the signal-to-noise ratio. However, counting times of several hours per detector position were still required to obtain statistically meaningful data.

X-ray diffraction data were collected at the National Synchrotron Light Source at the Brookhaven National Laboratory using beamline X20C. To reduce the background from the Si substrates, data were collected in a grazing incidence geometry. The diffracted beam was analyzed with 1 mrad Soller slits, which provided a finer resolution than any of the diffraction peak widths. To calculate the grain size distribution of the FePt particles, the entire XRD data set was fitted to a model where the peak shapes contain contributions from nonuniform strain and grain size broadening.<sup>28</sup> The shape of each diffraction peak was then a convolution of the shapes due to grain-size broadening, which was assumed to originate from a lognormal distribution of grain sizes,<sup>29,30</sup> and to nonuniform strain, which was assumed to be Gaussian:

$$I(Q) = \int_0^\infty P(Q,d) \frac{\exp\left(\frac{-(d-d_0)^2}{2\sigma_d^2}\right)}{\sqrt{2\pi}\sigma_d} dd. \quad (1)$$

Here  $Q$  is the scattering vector,  $d$  is the plane spacing,  $d_0$  is the average plane spacing,  $\sigma_d$  is the root-mean-square width of the Gaussian  $d$ -spacing distribution, and  $P(Q,d)$  is the shape for a lognormal distribution of grain sizes [Eqs. (6) and (15) in Ref. 30 with  $Q=2\pi s$ ]. For simplicity, the lognormal width ( $\sigma_{d-\ln}$ ) was fixed at 0.5. In all cases, when  $\sigma_{d-\ln}$  was allowed to vary, it converged to a value close to 0.5.

In a binary alloy, such as FePt, the extent of chemical order is quantified by the generalized Bragg-Williams long-range order parameter:

$$S = r_{\text{Fe}} + r_{\text{Pt}} - 1 = \frac{(r_{\text{Pt}} - x_{\text{Pt}})}{y_{\text{Fe}}} = \frac{(r_{\text{Fe}} - x_{\text{Fe}})}{y_{\text{Pt}}}. \quad (2)$$

Here  $x_{\text{Fe}}$  and  $x_{\text{Pt}}$  are the atom fractions of Fe and Pt, respectively,  $r_{\text{Fe}}$  and  $r_{\text{Pt}}$  are the fraction of Fe and Pt sites occupied by the correct atom in the  $L1_0$  structure; and  $y_{\text{Fe}}$  and  $y_{\text{Pt}}$  are the fractions of Fe and Pt sites, 0.5 for the  $L1_0$  phase (see Cebollada *et al.*<sup>31</sup> or Warren<sup>28</sup> for details). When the chemical order is perfect, each alternating layer perpendicular to the  $c$  axis is fully occupied by Fe or Pt atoms (i.e., all the Fe sites are occupied by Fe atoms and Pt sites by Pt atoms) and  $S=1$ . For complete chemical disorder, all sites are equally occupied by Fe and Pt and  $S=0$ . For partial chemical order,  $S$  is proportional to the number of atoms on correct sites ( $r_{\text{Fe}} + r_{\text{Pt}}$ ). The discussion above is applicable to homogeneous materials, but a material can be inhomogeneous, consisting

of regions that have high chemical order and regions that are nearly disordered (e.g., a two-phase system). This distinction between the microstructures suggests that an additional factor is needed to quantify chemical order in inhomogeneous materials. This factor is the volume fraction of the film that is chemically ordered, which we call  $f_0$ . In the case of inhomogeneous materials, we can then include  $f_0$ ,  $S_{\text{order}}$  ( $S$  in the chemically ordered regions), and  $S_{\text{ave}}$  (the volume averaged  $S$ ) as parameters in the data analysis. This is important as the nanoparticle assemblies (as with thin films<sup>32</sup>) are, in fact, inhomogeneous.

In order to calculate  $S_{\text{order}}$ ,  $f_0$ , and  $S_{\text{ave}}$ , we use the ratio of the integrated intensities of the various diffraction peaks corrected for the Lorentz-polarization factor, illuminated area, and the Debye-Waller parameter.<sup>28,33,34</sup>  $S_{\text{order}}$  is calculated from the ratio of the corrected integrated intensities of the  $L1_0$  (110) and (220) peaks. The ordered fraction,  $f_0$ , is determined from the fitted intensities of the fcc(220) together with the  $L1_0$  (202) and (220) peaks;  $f_0$  is the ratio of the  $L1_0$  peaks to the sum of the three peak intensities. The average chemical order  $S_{\text{ave}}$  is the product of  $S_{\text{order}}$  and  $f_0$ . As a check, and to improve the accuracy of the analysis,  $S_{\text{ave}}$  was also determined from the ratio of the  $L1_0$  (110) peak to the sum of the fcc(220) and  $L1_0$  (202) and (220) peaks. An explicit, detailed discussion of this procedure is given in Cebollada *et al.*<sup>31</sup>

### III. SIMULATIONS OF SANS DATA

In principle, small angle neutron scattering gives information on both nuclear and magnetic scattering potentials. The nuclear and magnetic contributions sum to give the total measured intensity as a function of scattering vector  $\mathbf{q}$ , where  $|\mathbf{q}|=4\pi \sin(\theta)/\lambda$ . In the case of a magnetically saturated sample the total intensity is given by<sup>35,36</sup>

$$I(\mathbf{q}) = I_N(\mathbf{q}) + [1 - (\hat{\mathbf{h}} \cdot \hat{\mathbf{q}})^2] I_M(\mathbf{q}), \quad (3)$$

where  $\hat{\mathbf{h}}$  and  $\hat{\mathbf{q}}$  are unit vectors in the magnetization and scattering directions respectively, and  $I_N(\mathbf{q})$  and  $I_M(\mathbf{q})$  are determined by the  $q$ -dependent nuclear and magnetic scattering cross sections.

For simplicity we consider a distributed set of particles, each at positions  $\mathbf{r}_i$ , having a scattering potential  $U(\mathbf{r}-\mathbf{r}_i)$ . For nuclear scattering this is the nuclear scattering potential  $U_N(\mathbf{r}-\mathbf{r}_i)$  due to the residual strong interaction of the neutron with the nucleus, while for magnetic scattering this is the magnetic dipolar interaction  $U_M(\mathbf{r}-\mathbf{r}_i)$  between the neutron and the local spatially varying magnetic flux density. These individual contributions to the total intensity depend on the partial differential cross section  $d\sigma/d\Omega$  for each interaction, which is the number of neutrons scattered per second into unit solid angle, divided by the incident neutron flux. Primary data reduction includes a step which normalizes the scattering data to the incident flux, and hence to extract information from our scattering results we simulate  $d\sigma/d\Omega(\mathbf{q})$ . The partial differential cross section for a system of volume  $V$ , containing  $N_p$  particles where each particle contains many individual (either nuclear or magnetic) scattering centers can be written as<sup>37,38</sup>

$$\frac{d\sigma}{d\Omega}(\mathbf{q}) = \frac{1}{V} \left\langle \sum_{i=1}^{N_p} \sum_{i'=1}^{N_p} F_i(\mathbf{q}) F_{i'}^*(\mathbf{q}) e^{-i\mathbf{q}\cdot(\mathbf{r}_i - \mathbf{r}_{i'})} \right\rangle, \quad (4)$$

where the brackets indicate an average over the ensemble. The quantity

$$F_i(\mathbf{q}) = c \int U_i e^{-i\mathbf{q}\cdot\mathbf{r}} d^3\mathbf{r}, \quad (5)$$

often referred to as the *form factor*, is the Fourier transform of the local scattering potential,  $U_i$ , due to particles at  $\mathbf{r}_i$ , where the constant  $c$  depends on the nature of the interaction. We note that in the case of scattering from a spherically symmetric potential the Born approximation allows the form factor to be written as  $F_i(\mathbf{q}) = \int b_i e^{-i\mathbf{q}\cdot\mathbf{r}} d^3\mathbf{r}$  where the scattering length  $b_i$  is defined by  $\int_{\text{particle}} U_i(\mathbf{r}) d\mathbf{r} = (-2\pi\hbar^2/m)b_i$ .

We next separate scattering into intraparticle  $i=i'$  and interparticle  $i \neq i'$  contributions. For intraparticle scattering Eq. (4) gives

$$i = i': \frac{d\sigma}{d\Omega}(\mathbf{q}) = \frac{N_p}{V} \langle F^2(\mathbf{q}) \rangle. \quad (6)$$

In deriving the interparticle terms we consider a system in which there is no correlation between the values of the scattering potentials (e.g., particle size and/or orientation) and their positions. This is a reasonable assumption for self-assembled FePt nanoparticles with a relatively low packing fraction. Thus the interference term may be factorized as

$$i \neq i': \frac{d\sigma}{d\Omega}(\mathbf{q}) = \frac{1}{V} \sum_{i=1}^{N_p} \sum_{i'=1(i \neq i')}^{N_p} \langle F_i(\mathbf{q}) \rangle \langle F_{i'}^*(\mathbf{q}) \rangle \langle e^{-i\mathbf{q}\cdot(\mathbf{r}_i - \mathbf{r}_{i'})} \rangle \quad (7)$$

which leads to

$$i \neq i': \frac{d\sigma}{d\Omega}(\mathbf{q}) = \frac{N_p}{V} \langle F(\mathbf{q}) \rangle^2 H(\mathbf{q}), \quad (8)$$

where the pair correlation function is defined as

$$H(\mathbf{q}) = \frac{1}{N_p} \sum_{i=1}^{N_p} \sum_{i'=1(i \neq i')}^{N_p} \langle e^{-i\mathbf{q}\cdot(\mathbf{r}_i - \mathbf{r}_{i'})} \rangle. \quad (9)$$

Combining these two cases into a single expression gives

$$\frac{d\sigma}{d\Omega}(\mathbf{q}) = \rho \langle F(\mathbf{q})^2 \rangle + \rho \langle F(\mathbf{q}) \rangle^2 H(\mathbf{q}), \quad (10)$$

where the number density of the particles is defined as  $\rho = N_p/V$ .

The structure factor  $S(\mathbf{q})$  is related to the pair correlation function through  $S(\mathbf{q}) = 1 + H(\mathbf{q})$ , where  $S(\mathbf{q}) = (1/N_p) \sum_i \sum_{i'} \langle e^{-i\mathbf{q}\cdot(\mathbf{r}_i - \mathbf{r}_{i'})} \rangle$  and the double summation runs over all  $i, i'$ . Thus the scattering cross section can be written in terms of the structure factor as

$$\frac{d\sigma}{d\Omega}(\mathbf{q}) = \rho \langle F(\mathbf{q}) \rangle^2 S(\mathbf{q}) + \rho (\langle F^2(\mathbf{q}) \rangle - \langle F(\mathbf{q}) \rangle^2). \quad (11)$$

For amorphous arrangements of particles  $S(\mathbf{q})$  is well represented by the Percus-Yevick formula for interacting hard spheres<sup>39</sup> and describes the interference effects of scattering from different particles. This contains information about the local arrangement of particles relative to one another. The second term in Eq. (11) is effectively the correction to the first term of Eq. (10) to account for the fact that all particles in the system are not identical. For a set of identical particles equations (10) and (11) become

$$\frac{d\sigma}{d\Omega} = \rho \langle F(\mathbf{q}) \rangle^2 S(\mathbf{q}). \quad (12)$$

We now have a formalism for a dispersion of identical particles that includes the effects of interparticle interference. In the literature Eqs. (11) and (12) are frequently used to describe scattering from polydispersed and monodispersed systems of particles, respectively. In order to obtain a realistic model of the nanoparticle arrays the effects of a distribution of particles sizes must be included, and proper account should be taken of the interference terms. In terms of a distribution of particle sizes  $f(\sigma_m)$  of radius  $\sigma_m$  the differential cross-section (11) can be written as<sup>40,41</sup>

$$\begin{aligned} \frac{d\sigma}{d\Omega} = & \rho \int_0^\infty F_m^2(q) f(\sigma_m) d\sigma_m \\ & + \rho \int_0^\infty \int_0^\infty F_m(q) F_n(q) H_{mn}(q) f(\sigma_m) f(\sigma_n) d\sigma_m d\sigma_n. \end{aligned} \quad (13)$$

While for systems that are close to being monodispersed, Eqs. (10)–(12) are all reasonable approximations;<sup>41</sup> as the systems become more polydispersed it becomes necessary to properly account for the interparticle interference terms via Eq. (13). This is the approach we have used in this work. Even for the case of high polydispersity, in a densely packed system the use of Eq. (11) over Eq. (13) can lead to significant errors in simulating the data, since undue weight is given to particles of larger diameter. Equation (13) has been solved analytically in the Percus-Yevick approximation for the case of a particle size distribution give by a Schulz (gamma) distribution of diameters by Griffith *et al.*<sup>41</sup> The Schulz (gamma) distribution is given by

$$f(\sigma) = \frac{\sigma^{c-1} \exp(-\sigma/b)}{b^c \Gamma(c)}$$

where  $b = \sigma_{\text{mean}}/(z+1)$ ,

$$c = z + 1, \quad (14)$$

and  $z$  is the Schulz distribution width factor ( $z > -1$ ). The Schulz (gamma) distribution is chosen due to its mathematical tractability. This distribution has a functional form similar to that of a lognormal distribution and it is therefore

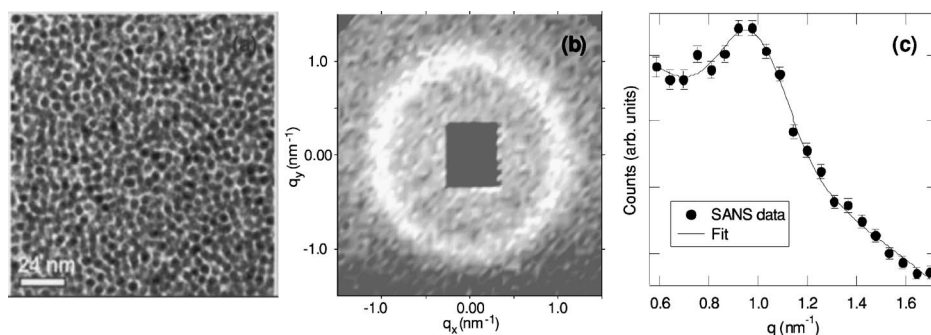


FIG. 1. (a) SEM, (b) SANS detector image, and (c) integrated SANS signal for a self-assembled unannealed nanoparticle array having a particle diameter of 4 nm and a spacing of 6.5 nm.

physically very reasonable to use this form to describe the size distribution of an assembly of particles.

We first consider the contribution from magnetic scattering. Since a field greater than 2 T is required to saturate our FePt nanoparticle assemblies it was not possible to align the particles magnetically with the available SANS experimental environment. Particles with a 3D random distribution of anisotropy axes give, in zero applied field, a magnetic contribution to scattering that is equal along all directions,  $\mathbf{q}$ . The magnetic contribution is proportional to  $\frac{1}{3}\langle M^2(\mathbf{q}) \rangle$ , where  $\langle M(\mathbf{q}) \rangle = \langle \int M(\mathbf{r}) e^{-i\mathbf{q} \cdot \mathbf{r}} d^3\mathbf{r} \rangle$  is the average value of the Fourier component of the local spatially varying magnetization  $M(\mathbf{r})$ , analogous to the form factor  $F(\mathbf{q})$  in the foregoing discussion. In order to separate out the magnetic contribution from the nuclear scattering, one can use the anisotropic contribution to the scattering due to the total or partial polarization of the magnetization, as indicated in Eq. (3). The magnetic scattering is suppressed along the direction in which the magnetization lies; for the case of a saturated magnetic sample, the magnetic scattering goes to zero along the direction of the applied magnetic field. We have used this technique to successfully extract the magnetic scattering from the thin films of continuous longitudinal recording media, where the diameters of the grains and film thickness are of similar dimensions to the FePt nanoparticle system considered here.<sup>42</sup> In the present work we attempted to evaluate the size of the magnetic signal relative to the nuclear scattering using the same approach. For applied fields of up to 1.3 T the anisotropic magnetic signal was not apparent in these samples, implying that even in zero field the scattering is dominated by the nuclear scattering due to the strong contrast in neutron scattering potential between the metallic particles and the organic matrix in which they are embedded. In the analysis which follows we assume that the scattering originates entirely from the nuclear cross section. In reality, since we are making all measurement in zero field on samples in the virgin magnetic state, and given that at these particle sizes the magnetic grain size is likely to closely resemble the physical grain size, then in modeling the dispersion of particle sizes such an assumption is not likely to unduly prejudice the distributions we obtain from the analysis.

Using the analytic solution of Griffith *et al.*<sup>41</sup> to Eq. (13) allowed an extensive series of simulations to be undertaken to investigate the effect of the various parameters on the simulated data. These simulation experiments showed that the interference term was relatively unimportant in determin-

ing the  $\mathbf{q}$  dependence of the scattering intensity for the particle concentration of the assemblies investigated here where the volume fraction is 0.13.<sup>39</sup> Attempts to simulate the experimental data using a single Schulz (gamma) distribution produced a reasonable fit to the data. However, the refinement of including a second distribution function improved the quality of the fit, and since for wide distributions incoherent scattering strongly reduces the relative contribution of the particle-particle interference term, this refinement does not introduce significant errors. The error bars on the data sets are such that some small changes in the functional form of the particle diameter distribution do not affect the quality of the fit, provided that the median particle diameter and the distribution width remain the same. Thus while the precise details of the particle diameter distribution are subject to some small uncertainties the overall functional form can be accurately simulated. In order to check the validity of our simulations a polydisperse model of interacting particles proposed by Kotlarchyk *et al.*<sup>37</sup> was tested. Simulations using both models produced very similar results for identical input parameters. Simulations using only a distribution of hard sphere diameters were also attempted. Again input parameters, appropriate to the nanoparticle assemblies studied here, generated similar scattering intensities. This indicates that the interference terms do not contribute significantly to the total scattered intensity for assemblies with the packing fractions and wide distributions considered here.

#### IV. RESULTS AND DISCUSSION

Figure 1(a) shows a scanning electron microscope (SEM) image of an as-deposited nanoparticle assembly. Figure 1(b) is an image of the SANS detector ( $64 \times 64$  element) showing the data with the normal instrumentation corrections. It is immediately apparent that there is significant coherent scattering from the particles giving rise to the observed ring. The interference terms in the scattering leads to a  $S(q)$  which cause the scattering intensity to peak at  $|q| \sim 2\pi/d$ , where  $d$  is the nearest-neighbor separation. An estimate of the position of this peak was obtained by azimuthally integrating around the detector and fitting to a Gaussian function. This yielded a peak at  $|q| \approx 1.0 \text{ nm}^{-1}$  corresponding to a nanoparticle plane spacing,  $d$ , of  $6.4 \text{ nm} \pm 0.1 \text{ nm}$ , in excellent agreement with the particle periodicity found from TEM and SEM images.<sup>25</sup> The fact that the scattering involves a  $S(q)$ , with a width equivalent to 1.2 nm in real space, rather than sharp Bragg peaks indicates that long range order does not extend

over the entire coherence length of the neutrons. The lack of long range orientational order is also indicated by the fact that peak intensity is evenly distributed around a ring on the detector. This absence of both spatial and orientational order over large areas is clearly a limitation of self-assembled arrays which might be addressed by depositing the nanoparticles onto prepatterned substrates such that perfectly ordered arrays are only required over a few microns. These data were analyzed in more detail using the Griffith model where a particle diameter of 4.0 nm was obtained assuming a packing fraction of 0.13 and a particle separation of 6.5 nm, in agreement with the simple analysis presented above. These values are also consistent with results obtained on similar particle assemblies studied using SEM and TEM where particle diameters of 4 nm with a narrow distribution of sizes were observed.<sup>1</sup> In contrast, performing a detailed analysis of the Bragg peaks in the XRD data, as described above, a crystallographic, volume averaged particle diameter of 2.2 nm is obtained.<sup>43</sup> These differences can be explained by considering the different physical effects being probed. XRD is sensitive to coherent planes of atoms *within the particle* whereas SANS is sensitive only to particle sizes, shapes, and *inter-particle* correlations, and SEM/TEM requires a large electron scattering contrast. Hence combining the different sensitivities of SANS and XRD allows a more complete physical description of these nanoparticle systems than either technique could provide in isolation. The data suggest a model where particles consist of a well-defined metallic core surrounded by a shell of amorphous material. This model is also strongly supported by magnetization and NEXAFS data.<sup>43,44</sup> Measurements of magnetization vs applied field as a function of temperature show that the unannealed arrays are superparamagnetic and that the data are well-described by a Langevin function where the saturation magnetization is 1030 emu/cm<sup>3</sup>, which is the value for disordered fcc FePt, and a particle diameter of 2.2 nm. NEXAFS results show that the as-deposited particles have very little spectral intensity due to Fe in a metallic environment and that the observed signal can be modeled as originating from Fe oxide. Due to the escape depth of secondary electrons, the atoms at the surface of a particle are largely responsible for the observed signal as discussed in detail by Anders *et al.*<sup>44</sup> Hence we are now able to understand the physical state of the unannealed nanoparticles in terms of a metallic, magnetically active core of diameter 2.2 nm surrounded by a non-magnetic, or only very weakly magnetic, shell. This model of as-deposited nanoparticle arrays will then act as a starting point in order to understand the annealing process.

In order to investigate the evolution of nanoparticle assemblies with annealing we have measured the magnetic and structural properties as a function of annealing temperature. Changes in magnetic properties have already been reported<sup>43</sup> and here we concentrate on structural aspects. Figure 2 shows SANS data and simulations which include a small constant background term, together with the distributions of particle diameters used to produce the simulations, as a function of annealing temperature. In the case of the sample annealed under the 700 °C/5 min condition, the particle diameters increased to a size which gave scattering at *q* values lower than those accessible experimentally. Hence for this

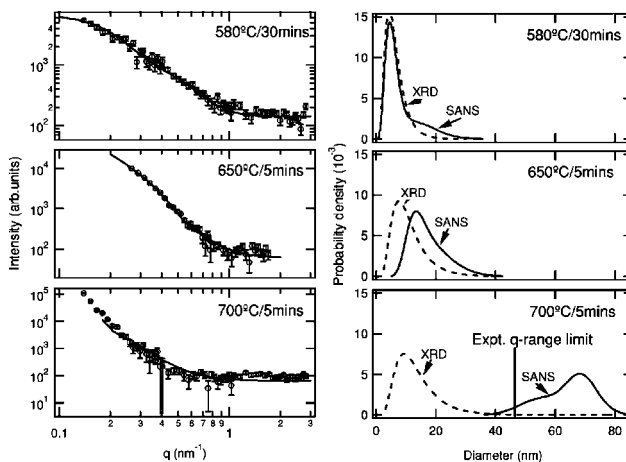


FIG. 2. SANS data and simulations for FePt nanoparticle assemblies for a variety of annealing conditions: 580 °C/30 min, 650 °C/5 min, and 700 °C/5 min. The corresponding particle size distributions obtained from the simulations (solid lines) together with the particle size distribution estimated from XRD data (dashed lines) are shown opposite. Note that the size distribution obtained from the SANS data for the 700 °C/5 min annealing condition is subject to greater uncertainty since experimentally the corresponding *q* range was not completely measured as shown in the figure.

sample the distribution of diameters, obtained from simulations of the data, set a lower bound on the particle size distribution rather than providing full information on the distribution. The limit of the data is marked in Fig. 2. Also shown are the distributions of particle diameters determined from XRD measurements using the analysis method described above. These data are summarized in Fig. 3 where the median diameters and width of the particle size distributions are plotted. These results immediately show that even at the lowest anneal temperature required to produce significant coer-

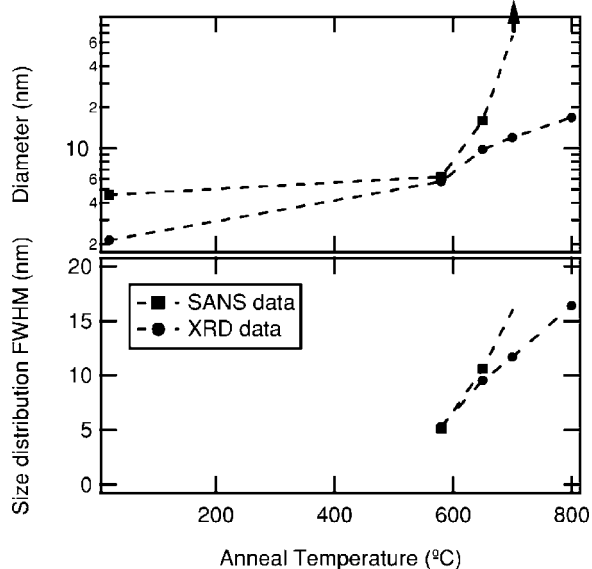


FIG. 3. Summary of particle diameters and the full width at half maximum of the particle size distributions obtained from SANS and XRD results. The dotted lines are included as a guide to the eye.

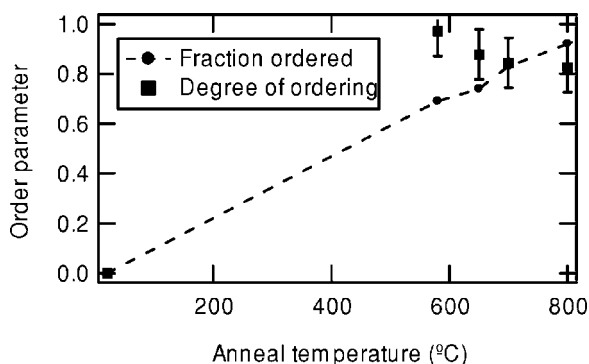


FIG. 4. Fraction of particles with  $L1_0$  ordering and the degree of ordering within this fraction as a function of anneal temperature. The data show that a two state model, where particles are either not ordered or are essentially fully ordered should be used to describe these nanoparticle arrays. The dotted line is included as a guide to the eye.

civity at room temperature we observe both agglomeration and sintering. The two techniques also demonstrate a significant distribution of particles sizes with the SANS data giving a tail of large diameter particles for the 580 °C/30 min anneal condition. At higher annealing temperatures the distribution of diameters and the median diameter obtained from the SANS measurement increases rapidly. The particle diameters obtained from the x-ray analysis also increase substantially. Since the width of the x-ray peaks forms the basis of the particle size analysis, it follows that the x-ray measurement is sensitive only to coherent lattice planes. Hence annealing the particles results in an x-ray diameter greater than the initial particle size and we associate the increased diameter with particle sintering where particles combine to form a larger entity with a common crystallographic axis.

Figure 4 shows  $L1_0$  ordering in these particles. As mentioned in the previous section it is important to note that, in common with many  $L1_0$  materials, the chemical ordering in these nanoparticles is inhomogeneous: there are regions that are chemically ordered and regions that are chemically disordered. The extent of order within the ordered regions is shown by the squares in Fig. 4, while the fraction of the assembly that is chemically ordered is shown by the circles. With this in mind, the data in Fig. 4 demonstrate that chemical ordering in particle assemblies has two components. First, the degree of ordering within the population of particles that are ordered, which shows that such particles are close to being fully ordered. Second, the fraction of particles

that are ordered, which increases from 60% for the 580 °C/30 min anneal condition to 90% for the 800 °C/5 min treatment. We note that a commensurate increase in coercivity with the fraction of particles that are ordered from 9.8 to 36.9 kOe (measured at  $T=20$  K) has also been found.<sup>43</sup> Thus even after annealing at the highest temperature for 5 min, not all particles are chemically ordered despite the fact that severe agglomeration has already occurred. These results on ordered fractions show a potentially severe limitation in using FePt nanoparticles as a recording medium, since any high density recording scheme is likely to demand a medium that has uniform properties.

## V. CONCLUSION

We have demonstrated the utility of combining SANS measurements with XRD to gain an understanding of the physical structure of nanoparticle assemblies. In this way we are able to separate the effects of particle sintering from those of agglomeration. We provide evidence that unannealed particles consist of a metallic, magnetic core surrounded by an oxide containing shell, consistent with magnetization data reported previously.<sup>43</sup> The data show that annealing leads to a large change in the median particle size and that a large distribution of particle sizes exists. The data also provide evidence that to first order the macroscopic magnetic properties of the assemblies are not dependent on the particle sizes but depend instead on the fraction of particles with  $L1_0$  ordering,  $f_0$ . The work clearly demonstrates that if nanoparticle arrays are to become a viable recording technology where data is stored one bit per particle, then the problem of particle sintering and agglomeration must be addressed. However, the promise of storage densities above 1 Tbit/in.<sup>2</sup> provides a strong incentive for future research in FePt nanoparticles and ensures that this will continue to be an active area of endeavor.

## ACKNOWLEDGMENTS

This research was carried out in part at the National Synchrotron Light Source, Brookhaven National Laboratory, which is supported by the U.S. Department of Energy, Division of Materials Sciences and Division of Chemical Sciences, under Contract No. DE-AC02-98CH10886. Portions of this research were carried out at the Stanford Synchrotron Radiation Laboratory, a user facility operated by Stanford University on behalf of the U.S. Department of Energy, Office of Basic Energy Sciences.

<sup>1</sup>S. Sun, C. B. Murray, D. Weller, L. Folks, and A. Moser, *Science* **287**, 1989 (2000).

<sup>2</sup>H. Zeng, J. Li, J. P. Liu, Z. L. Wang, and S. Sun, *Nature (London)* **420**, 395 (2002).

<sup>3</sup>Q. A. Pankhurst, J. Connolly, S. K. Jones, and J. Dobson, *J. Phys. D* **36**, R167 (2003).

<sup>4</sup>S. Kang, J. W. Harrell, and D. E. Nikles, *Nano Lett.* **2**, 1033

(2002).

<sup>5</sup>S. Stappert, B. Rellinghaus, M. Acet, and E. F. Wassermann, *J. Cryst. Growth* **252**, 440 (2003).

<sup>6</sup>T. Hyeon, *Chem. Commun. (Cambridge)* **8**, 927 (2003).

<sup>7</sup>B. Jeyadevan, K. Urakawa, A. Hobo, N. Chinnasamy, K. Shinoda, K. Tohji, D. D. J. Djayaprawira, M. Tsunoda, and M. Takahashi, *Jpn. J. Appl. Phys., Part 2* **42**, L350 (2003).

- <sup>8</sup>Y. Huang, H. Okumura, G. C. Hadjipanayis, and D. Weller, *J. Magn. Magn. Mater.* **242–245**, 317 (2002).
- <sup>9</sup>T. J. Klemmer, N. Shukla, C. Liu, X. W. Wu, E. B. Svedberg, O. Mryasov, R. W. Chantrell, D. Weller, M. Tanase, and D. E. Laughlin, *Appl. Phys. Lett.* **81**, 2220 (2002).
- <sup>10</sup>Z. R. Dai, S. Sun, and Z. L. Wang, *Surf. Sci.* **505**, 325 (2002).
- <sup>11</sup>B. Stahl, J. Ellrich, R. Theissmann, M. Ghafari, S. Bhattacharya, H. Hahn, N. S. Gajbhiye, D. Kramer, R. N. Viswanath, J. Weissmüller, and H. Gleiter, *Phys. Rev. B* **67**, 014422 (2003).
- <sup>12</sup>G. V. Kuryandskaya, M. L. Sanchez, B. Hernando, V. M. Prida, P. Gorria, and M. Tejedor, *Appl. Phys. Lett.* **82**, 3053 (2003).
- <sup>13</sup>D. K. Kim, M. Mikhaylova, Y. Zhang, and M. Muhammed, *Chem. Mater.* **15**, 1617 (2003).
- <sup>14</sup>F. Scherer, M. Anton, U. Schillinger, J. Henke, C. Bergemann, A. Kruger, B. Gansbacher, and C. Plank, *Gene Ther.* **9**, 102 (2002).
- <sup>15</sup>S. Sun, D. Weller, and C. B. Murray, in *The Physics of Ultra-High-Density Magnetic Recording*, edited by M. L. Plumer, J. van Ek, and D. Weller (Springer, New York, 2001).
- <sup>16</sup>S. Anders, M. F. Toney, T. Thomson, J.-U. Thiele, R. F. C. Farrow, B. D. Terris, S. Sun, and C. B. Murray, *J. Appl. Phys.* **93**, 6299 (2003).
- <sup>17</sup>J. W. Harrell, S. Wang, D. E. Nikles, and M. Chen, *Appl. Phys. Lett.* **79**, 4393 (2001).
- <sup>18</sup>X. W. Wu, K. Y. Guslienko, R. W. Chantrell, and D. Weller, *Appl. Phys. Lett.* **82**, 3475 (2003).
- <sup>19</sup>R. W. Chantrell, D. Weller, T. J. Klemmer, S. Sun, and E. E. Fullerton, *J. Appl. Phys.* **91**, 6866 (2002).
- <sup>20</sup>E. Mayes, A. Bewick, D. Gleeson, J. Hoinville, R. Jones, O. Kasuyutich, A. Nartowski, B. Warne, J. Wiggins, and K. K. W. Wong, *IEEE Trans. Magn.* **39**, 624 (2003).
- <sup>21</sup>D. Weller and A. Moser, *IEEE Trans. Magn.* **35**, 4423 (1999).
- <sup>22</sup>X. Sun, S. Kang, J. W. Harrell, D. E. Nikles, Z. R. Dai, J. Li, and Z. L. Wang, *J. Appl. Phys.* **93**, 7337 (2003).
- <sup>23</sup>S. S. Kang, D. E. Nikles, and J. W. Harrell, *J. Appl. Phys.* **93**, 7178 (2003).
- <sup>24</sup>J. W. Harrell (private communication).
- <sup>25</sup>S. Sun, S. Anders, H. F. Hamann, J.-U. Thiele, J. E. E. Baglin, T. Thomson, E. E. Fullerton, C. B. Murray, and B. D. Terris, *J. Am. Chem. Soc.* **124**, 2884 (2002).
- <sup>26</sup>S. Sun, S. Anders, T. Thomson, J. E. E. Baglin, M. F. Toney, H. F. Hamann, C. B. Murray, and B. D. Terris, *J. Phys. Chem. B* **107**, 5419 (2003).
- <sup>27</sup>P. Lindner, R. P. May, and P. A. Timmins, *Physica B* **180&181**, 967 (1992).
- <sup>28</sup>B. E. Warren, *X-Ray Diffraction* (Addison-Wesley, Reading, MA, 1969).
- <sup>29</sup>W. L. Prater, E. L. Allen, W.-Y. Lee, M. F. Toney, J. Daniels, and J. A. Hedstrom, *Appl. Phys. Lett.* **84**, 2518 (2004).
- <sup>30</sup>N. C. Poppa and D. Balzar, *J. Appl. Crystallogr.* **35**, 338 (2002).
- <sup>31</sup>A. Cebollada, R. F. C. Farrow, and M. F. Toney, in *Magnetic Nanostructures*, edited by H. S. Nalva (American Scientific Publishers, Stevenson Ranch, 2002), p. 93.
- <sup>32</sup>M. F. Toney, W. Y. Lee, J. A. Hedstrom, and A. Kellock, *J. Appl. Phys.* **93**, 9902 (2003).
- <sup>33</sup>R. F. C. Farrow, D. Weller, R. F. Marks, M. F. Toney, S. Hom, G. R. Harp, and A. Cebollada, *Appl. Phys. Lett.* **69**, 1166 (1996).
- <sup>34</sup>M. F. Toney and D. G. Wiesler, *Acta Crystallogr., Sect. A: Found. Crystallogr.* **A49**, 624 (1993).
- <sup>35</sup>D. J. Cebula, S. W. Charles, and J. Popplewell, *Colloid Polym. Sci.* **259**, 395 (1981).
- <sup>36</sup>G. Kostorz, in *Treatise on Materials Science and Technology Vol. 15: Neutron Scattering*, edited by G. Kostorz (Academic, New York, 1979).
- <sup>37</sup>M. Kotlarchyk and S.-H. Chen, *J. Chem. Phys.* **79**, 2461 (1983).
- <sup>38</sup>S. W. Lovesey, *Theory of Neutron Scattering from Condensed Matter* (Clarendon, Oxford, 1986), Vol. 1.
- <sup>39</sup>J. K. Percus and G. J. Yevick, *Phys. Rev.* **110**, 1 (1958).
- <sup>40</sup>W. L. Griffith, R. Triolo, and A. L. Compere, *Phys. Rev. A* **33**, 2197 (1986).
- <sup>41</sup>W. L. Griffith, R. Triolo, and A. L. Compere, *Phys. Rev. A* **35**, 2200 (1987).
- <sup>42</sup>S. L. Lee, T. Thomson, F. Y. Ogrin, C. Oates, M. Wismayer, C. Dewhurst, R. Cubitt, and S. Harkness, *MRS Symposia Proceedings No. 803* (Materials Research Society, 2004), GG4.4.1.
- <sup>43</sup>T. Thomson, M. F. Toney, S. Raoux, S. L. Lee, S. Sun, C. B. Murray, and B. D. Terris, *J. Appl. Phys.* **96**, 1197 (2004).
- <sup>44</sup>S. Anders, M. F. Toney, T. Thomson, J.-U. Thiele, B. D. Terris, S. Sun, and C. B. Murray, *J. Appl. Phys.* **93**, 7343 (2003).